Development of SiO2-coumarin fluorescent nanohybrid and its application for Cu(II) sensing in aqueous extracts of roadside soil

J Nanopart Res (2022) 24: 114
https://doi.org/10.1007/s11051-022-05492-6

RESEARCH PAPER

Development of SiO_2-coumarin fluorescent nanohybrid and its application for Cu(II) sensing in aqueous extracts of roadside soil

Bin Qian · Shamali De Silva · Suzie M. Reichman · Lei Bao · Adrian Trinchi · Minbo Lan · Gang Wei · Linda Váradi · Ivan Cole

Received: 9 February 2022 / Accepted: 10 May 2022 / Published online: 31 May 2022

Abstract A SiO_2-coumarin nanohybrid was investigated for its Cu(II) sensing performance in aqueous media, and in comparison with the Cu(II)-selective coumarin used alone. Fluorescence of both coumarin itself and the nanohybrid, $\lambda_{ex}/\lambda_{em}$ 435/481 nm, was selectively quenched by Cu(II) when tested against a range of multivalent cations. The nanohybrid had enhanced Cu(II) sensing properties when compared to the coumarin including (i) improved limit of detection from µM-level (0.48 µM) of Cu(II) using coumarin alone to nM-level (0.033 µM) and (ii) an extended linear detection range of 0.033–260 µM (0.0005–4.1 mg/mL) Cu(II) compared to 0.48–55 µM for the coumarin itself. The lower limit of detection and extended range were achieved with a smaller amount of coumarin and no traces of organic solvents used to help coumarin dissolution. Characterization suggested that under applied test conditions at pH = 5, SiO_2 nanoparticles with negative surface charges adsorbed coumarin and then (when present) Cu(II) ions. The SiO_2-coumarin nanohybrid was then applied for the determination of Cu(II) levels in aqueous soil extracts reaching over 94% recovery rates when used against the standard soil analysis method by inductively coupled plasma mass spectrometry (ICP-MS).

Keywords Coumarin · SiO_2 nanoparticles · Fluorescence · Cu(II) sensing · Soil sensing

Supplementary Information The online version contains supplementary material available at https://doi.org/10.1007/s11051-022-05492-6.

B. Qian (✉) · S. De Silva · L. Bao · L. Váradi (✉) · I. Cole
School of Engineering, RMIT University, GPO Box 2476, Melbourne, VIC 3001, Australia
e-mail: bin.qian0218@hotmail.com

L. Váradi
e-mail: linda.varadi@rmit.edu.au

S. M. Reichman
Centre for Anthropogenic Pollution Impact and Management (CAPIM), University of Melbourne, Melbourne, VIC 3010, Australia

S. M. Reichman
School of Biosciences, University of Melbourne, Melbourne, VIC 3010, Australia

A. Trinchi
CSIRO Manufacturing, Bayview Avenue, Clayton, VIC 3169, Australia

M. Lan
Shanghai Key Laboratory of Functional Materials, School of Chemistry and Molecular Engineering, East China University of Science and Technology, 130 Meilong Road, Shanghai 200237, China

G. Wei
CSIRO Mineral Resources, PO Box 218, Lindfield, NSW 2070, Australia

Introduction

Copper is an essential trace element that plays a significant role in biological and environmental applications. In the human body, Cu(II)- and Cu(II)-dependent enzymes are involved in critical biological processes to ensure normal cellular function (Grasso et al. 2013; Domaille et al. 2010). However, excessive copper intake can lead to imbalance and harmful effects in living organisms (Hao et al. 2015; Zhang et al. 2014). In animals and humans, Cu(II) has been shown to have a role in the development of neurodegenerative disorders such as Menkes, Wilson's, and Alzheimer's diseases, and influence the development of certain cancers (Ge et al. 2021). Copper exposure can occur via contamination of soil and drinking water originating mostly from human activities, such as corrosion (Jakeria et al. 2021; Tang et al. 2021), mining, or lackadaisical waste management practices. Thus, easy-to-use, affordable, and sustainable sensing methods for Cu(II) are highly sought after in clinical, food/water, and environmental industries (Ji et al. 2017; Zhu et al. 2012). In addition, the allowable Cu(II) is highly regulated in many environmental media, such as in soil (e.g. 100 mg/kg in Australia) (He et al. 2015) and drinking water (e.g. 2.0 mg/mL in Australia) (Tang et al. 2021; Seeley et al. 2013).

Among existing sensing techniques, optical sensing using colorimetric or fluorescent molecular probes is readily available and non-expensive tool for the analysis of liquid samples and dissolved Cu(II) levels. An often employed sub-class of fluorescent chemosensors for Cu(II) (Zhang et al. 2014; Ramdass et al. 2017; Sivaraman et al. 2018) sensing are coumarin derivatives (Kraljević et al. 2016; Seo et al. 2011) due to their sufficient photostability, tuneable sensitivity, and selectivity (Geißler et al. 2005; Li et al. 2019). For example, hydrazine derivative **1** was developed as a "turn-on" fluorescent probe for the detection of Cu(II) in aqueous acetonitrile with a limit of detection (LOD) of 0.058 μM (Table 1) (Zhang et al. 2019). In comparison, the coumarin-*N*-acylhydrazone derivative **2** was utilized for both colorimetric and fluorometric detection of Cu(II) in CH_3CN/H_2O (v/v, 9/1) with a LOD of 8 μM (Table 1) (Li et al. 2019). While there are a large number of fluorescent probes reported for the sensing of particular metal ions in solution, and despite their satisfactory selectivity, they are often limited by insufficient water solubility reducing their ease of use and applicability for environmentally friendly, on-site sensing (Huang et al. 2014; Wang et al. 2016) Another limiting factor is their inability to selectively distinguish the copper cations from a mixture containing multiple metal cations with similar electronic properties, such as in the case of soil extracts.

One way to overcome mentioned shortfalls is to use nanomaterials that can be surface modified with molecular probes, and that facilitates the dispersion of analyte-selective dyes in aqueous solutions while preserving the sensing performance, especially selectivity (Lin et al. 2006). Such approaches often result in improvements in the limit of detection (LOD) due to the changes in surface to mass ratio of the hybrid sensing materials (Meiling and Guowen 2017) Among others, SiO_2 nanoparticles (SiO_2 NPs) are water dispersible and non-toxic with well-established, facile synthesis methods via, for example, the the Stöber method (Stöber et al. 1968). A previously reported combination using negatively charged SiO_2 NPs and

Table 1 Examples of fluorescent Cu(II) sensors and their reported excitation and emission wavelengths, and limits of detection in given solvents

	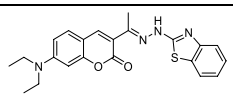	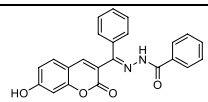	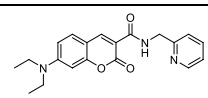	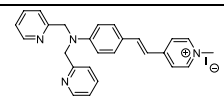
	1	**2**	**3**	**4**
λ_{ex} (nm)	376	309	435	365
λ_{em} (nm)	465	472	481	575
LOD (μM)	0.058	8	0.5	0.0112
Solvent	MeCN/H_2O (v/v, 1/1)	CH_3CN/H_2O (v/v, 9/1)	DMSO/H_2O (v/v, 1/9)	PBS buffer

positively charged molecular probe **4** (Table 1) was demonstrated for its use as a metal ion sensor in aqueous media (Peng et al. 2018). The authors discussed that electrostatic interactions between the dye **4** and the SiO_2 NP surface resulted in a locally increased concentration of **4** while an enhancement of the fluorescence intensity was recorded. For Cu(II) in tap water, use of 0.25 mg/mL SiO_2-**4** was delivering a sensing range of 11.2–100 nM and an LOD of 0.2 nM, an improvement from the LOD of 10 µM when **4** was used alone (Peng et al. 2018). A fluorescent, covalently appended SiO_2-naphthalin sensor was also reported for Hg(II) detection with a sensing range of 0.1–1 µM and LOD of 6.8 nM in water between pH 4.5 and 8 (He et al. 2009).

The current study aimed to improve the aqueous dispersibility and Cu(II) sensing performance of previously reported coumarin **3** (Qian et al. 2019) by coupling to non-toxic SiO_2 NPs to form SiO_2-**3** nanohybrid. The aim of this work is for on-site, facile, low-cost measurements of water and soil quality that can be conducted by non-trained personnel.

Synthesis of coumarin **3**, SiO_2 NPs, and the SiO_2-**3** nanohybrid is described. Then relevant optical, physical, and chemical properties are discussed and compared for each material in aqueous media and in the absence and presence of Cu(II) and other metal ions. While the interaction of Cu(II) with coumarin **3** is well studied, here the focus is given to its interaction with SiO_2 NPs and Cu(II) to understand how these affect the observed sensing properties. Finally, the SiO_2-**3** nanohybrid was tested on aqueous extracts of soil samples and its Cu(II) sensing performance was validated against the industry standard, inductively coupled plasma mass spectrometry (ICP-MS) method.

Experiment

Materials and instrumentations

Ammonia solution (30%) was purchased from Chemsupply. Tetraethyl orthosilicate (TEOS, 99%), diethyl malonate (99%), piperidine (99.5%), 4-(diethylamino)-2-hydroxybenzaldehyde (AR), and trifluoroacetic acid (99%) were purchased from Sigma-Aldrich (USA). 2-(Aminomethyl) pyridine (99%) was obtained from Acros Organics (Belgium, USA). All chemicals were used as received without further purification. Benzotriazol-1-(yloxy)tripyrrolidinophosphonium hexafluorophosphate (PyBOP (PF^{6-})) was purchased from Oakwood Chemical (West Columbia, USA).

Infrared spectra were recorded on Nicolet 6700 FTIR (Thermo Scientific, USA). UV–vis and fluorescence spectra were measured on a Cary Eclipse 5G UV–Vis-NIR spectrometer and a Cary Eclipse fluorescence spectrophotometer (USA), respectively. Nuclear magnetic resonance and mass spectra were recorded on Bruker Ascend 400 Hz and Thermo Q Exactive in a high-resolution electrospray mode mass spectrometer, respectively. The SiO_2 NP separation process was conducted using an Eppendorf Mini Spin centrifuge. A Jeol 1010 TEM instrument was used for the imaging of SiO_2 NPs and SiO_2-**3** complex structure. Size distribution and surface charge were studied using a Malvern ZEN3600 Zetasizer instrument. Elemental analyses of the SiO_2 NP surface were characterized by X-ray photoelectron spectroscopy (Thermo Scientific K-Alpha XPS). Thermogravimetric analysis (TGA) was conducted on Mettler Toledo micro balances. ICP-MS (Agilent with laser ablation capability) was used for the quantification of metal ion concentration in soil extracts and ICP-OES (Varian Vista-Pro) was applied for the Cu(II) concentration before and after the interaction with SiO_2 NPs.

Synthesis of coumarin 3 and SiO_2 nanoparticles

Coumarin **3** (Table 1) was synthesized via coumaric acid precursors as previously published (Nielsen and Houlihan 2004) (and detailed in the Supporting Information), followed by amide bond formation using PyBOP as a coupling agent (Scheme SI 1). The moderate yield was counter balanced by a simple work-up procedure by the removal of water-soluble by-products (SI Scheme 1) (Qian et al. 2019). After the preparation of SiO_2 NPs via Stöber synthesis (Fors et al. 2013), the SiO_2-**3** nanohybrid was assembled as described in the "Experiment" section. The color of the as-received nanohybrid was yellow compared to the white SiO_2 NPs due to the presence of coumarin **3**.

Preparation of SiO_2-3 nanohybrid

The preparation of coumarin **3** and SiO_2 NPs can be found in the supporting information (SI 1.1–1.3). To assemble SiO_2-**3**, SiO_2 NP (50 mg) was mixed into an aqueous 250-μM suspension of **3** (100 mL). The pH was adjusted to 5 using 0.01 M hydrochloric acid, and the resulting mixture was incubated at 37 ℃ for 2 h while gently stirred. The SiO_2-**3** nanohybrid was separated from the mixture by centrifuging the solution at 13,000 rpm and decanting the liquid phase and retaining the supernatant. The resulting particles were washed with Milli-Q water (3 × 1.5 mL) and pH = 5 was adjusted using hydrochloric acid, to remove the non-adsorbed coumarins. The obtained nanohybrid solution was centrifuged at 13,000 rpm and dried in a vacuum oven at 50 °C.

Preparation of Cu(II), coumarin 3, and SiO_2-3 nanohybrid solutions for optical measurements

$CuCl_2$ dihydrate stock solution (1 mM) was prepared in Milli-Q water and used for further dilution as required. Coumarin **3** was dissolved in DMSO/HEPES buffer (1:9, v/v, 20 mM, pH = 5) at 80 μM. Then, 50 mg SiO_2-**3** nanohybrid was dissolved in 50 mL HEPES buffer (pH = 5) to form the stock solution.

Concentration dependence of fluorescence intensities

Fluorescence spectra of **3** (40 μM) was recorded at pH 5 at concentrations of 5–80 μM in DMSO/HEPES buffer (1:9, v/v, 20 mM, pH = 5) at λ_{ex} = 435 nm with slit width of 5 nm. Meanwhile, for the fluorescence intensity of SiO_2-**3** nanohybrid, the stock solution was diluted into the concentrations from 5 to 50 mg/L using HEPES buffer (20 mM, pH = 5) and tested using the same instrument settings.

pH dependence of fluorescence intensities

Fluorescence intensity of **3** (40 μM) and SiO_2-**3** nanohybrid (7.5 mg/L) at λ_{ex} = 435 nm with slit widths of 5 nm was recorded, respectively, across the pH range of 3–13, which was adjusted by 1 mmol NaOH and 1 mmol HCl solution.

Optical properties of coumarin 3, SiO_2 NP, and SiO_2-3 nanohybrid in the presence of various Cu(II) concentrations

Fluorescence spectra were recorded in the presence of $CuCl_2$ for **3** (40 μM) in DMSO/HEPES buffer (1:9, v/v, pH = 5, 20 mM) and SiO_2-**3** nanohybrid (7.5 mg/L) in HEPES buffer (pH = 5) at λ_{ex} = 435 nm with slit widths of 5 nm. The concentration of added $CuCl_2$ dihydrate was 0–80 μM for **3** and 0–260 μM for SiO_2-**3** nanohybrid. The fluorescence intensity of SiO_2 NPs (7.5 mg/L, pH = 5) was also recorded.

Quantitation of surface-adsorbed Cu(II) on SiO_2 NPs and SiO_2-3 nanohybrid by ICP-OES

A 30 mg/L stock solution of SiO_2 NPs (10 mL) was mixed with 300 μM $CuCl_2$ solution (10 mL) and then incubated at 37 ℃ for 2 h. The final concentration of SiO_2 NPs was 15 mg/L and Cu(II) concentration was 9.4 mg/L. Then, the SiO_2 NPs were separated from the mixture by centrifuging the solution at 13,000 rpm. The resulting solution (top layer) was sent to ICP-OES for the measurement of residual Cu(II) concentration. The same process was applied for the SiO_2-**3** nanohybrid.

Interference studies

Fluorescence intensity of SiO_2-**3** nanohybrid (7.5 mg/L) in HEPES buffer (20 mM, pH = 5) was recorded in the presence of selected metal chlorides, including Cu(II), Al(III), Ca(II), Cd(II), Co(II), Fe(III), Mn(II), Pb(II), Hg(II), Ni(II), Zn(II), Mg(II), Cu(I), and Fe(II); both in the absence and presence of $CuCl_2$ (80 μM) at λ_{ex} = 435 nm with slit width of 5 nm. A solution containing all these metal ions (200 μM each) was also prepared and fluorescence intensity of SiO_2-**3** nanohybrid was recorded under the same condition.

Cu(II) sensing in real soil samples

Surface soil samples were taken from roadsides in the west of Melbourne, Victoria, Australia. Each soil sample (2.5 g) was dispersed in water (25 mL) and shaken for 1 week to extract water-soluble constituents, including copper. The extracts were filtered through a nylon filter membrane with a pore size of 0.45 µm and analyzed for Cu using ICP-MS. The extracts were also measured for their Cu(II) concentration via fluorescence as described previously.

Results and discussion

Characterization of SiO_2 NPs and SiO_2-3 nanohybrid

Coumarin **3** is well-described in the literature, and its coordination with Cu(II) has been reported before (Qian et al. 2019; Jung et al. 2009). Based on the TEM images, both the SiO_2 NPs (Stöber et al. 1968) and the SiO_2-**3** nanohybrid showed spherical and apparently identical morphology with a particle diameter of around 100 nm (Fig. S9). The presence of coumarin **3** in the SiO_2-**3** nanohybrid was confirmed by XPS (Fig. 1). SiO_2 NPs both prior and after surface modification with coumarin **3** displayed characteristic peaks of C1s (285 eV), O1s (533 eV), Si2s (154 eV), and Si2p (103 eV), with the additional signal of N1s (~ 400 eV broad) appearing in the SiO_2-**3** nanohybrid, indicating the presence of **3**. (Note: During the synthesis process of SiO_2 NPs, there was only ammonia involved as N source which was fully removed by the washing and drying process.)

Next, ATR-FTIR spectra of both SiO_2 and SiO_2-**3** nanohybrid were recorded in solid state (Fig. 2, Fig. S10), where additional peaks originating from coumarin **3** (Fig. S7) were observed in the spectra of the SiO_2-**3** nanohybrid: stretching vibration of coumarin carbonyl group (1698 cm^{-1}), pyridine C-N (1617 cm^{-1}), amide N–H (1543 cm^{-1}), and -C = C- bond in pyridine (1419 cm^{-1}).

Comparison of the thermogravimetric analysis (TGA) curves recorded for SiO_2-**3** nanohybrid (black line) and SiO_2 NPs (red line) at a heating rate of 5 °C/min (Fig. 3) provided approximation of the quantity of surface-adsorbed coumarins as **3** has a lower decomposition temperature than SiO_2 NPs. For the SiO_2-**3** nanohybrid, weight loss of 18% (100 to 82%) was observed between room temperature to about 200 °C, attributed to the evaporation of physically bound water (Tham et al. 2020). Beyond, the SiO_2-**3** nanohybrid displayed 7.0% weight loss (82 to 75%) in the range from 200 to 450 °C which may be correlated to the combination of the SiO_2 NP surface functional groups degrading (mainly $-OC_2H_5$ and –OH (Zhuravlev 2000)) amounting to 3% (based on the SiO_2 NP TGA, 88 to 85%) and the amount of the surface bound coumarin **3** of 4% (7 to 3%). This allows for a coarse comparison between the loading capacity of the SiO_2-**3** nanohybrid and their fluorescence versus the use of the standalone coumarin **3**. This means when 7.5 mg/L SiO_2-**3** nanohybrid is used in the experiments, the

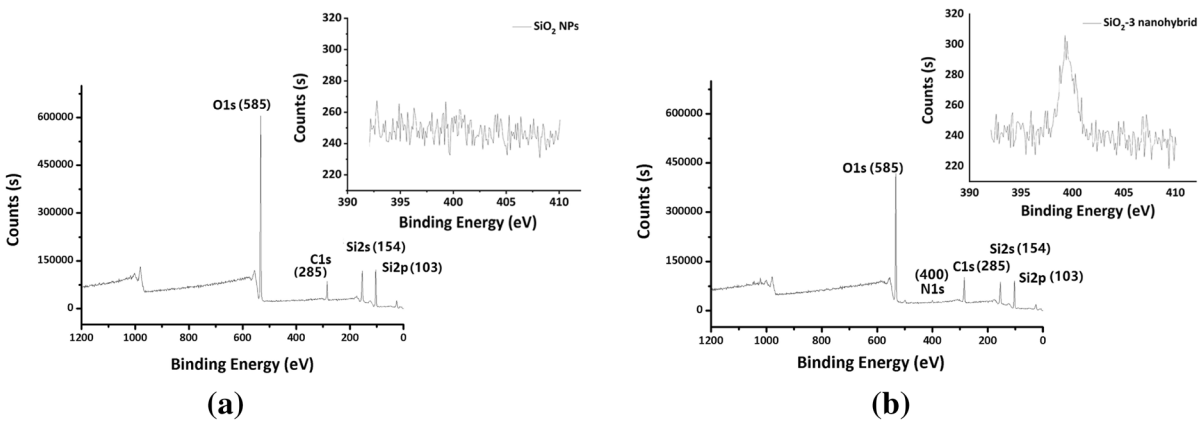

Fig. 1 XPS spectra of (**a**) SiO_2 NPs and insert: N1s scan of SiO_2 NPs and (**b**) SiO_2-**3** nanohybrid and insert: N1s scan of SiO_2-**3** nanohybrid

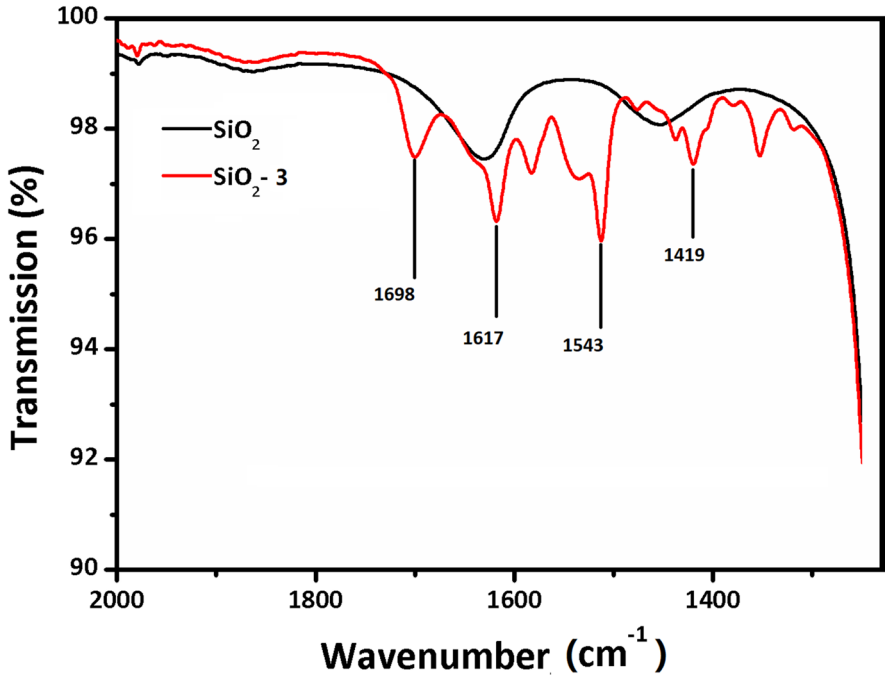

Fig. 2 ATR-FTIR spectra of SiO_2 NPs and SiO_2-**3** nanohybrid in the 2000–1300 cm^{-1} range

concentration of **3** will be about 0.8 µM but instead of an even distribution of coumarin **3** in the whole solution, now it would be adsorbed and concentrated on the surface of SiO_2 NPs. This localized **3** concentration increase would then expectedly lead to changes in optical properties.

Zeta potential of the SiO_2 NPs was − 30.5 mV (7.5 mg/L in HEPES buffer, 20 mM, pH 5) due

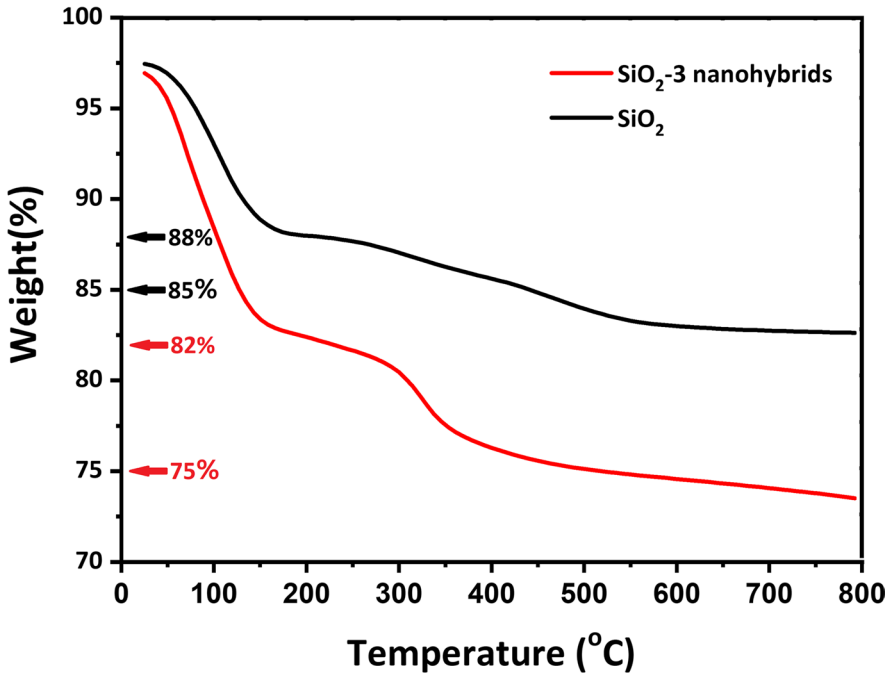

Fig. 3 Thermogravimetric analysis of SiO_2 NPs and SiO_2-**3** nanohybrid

to the abundant and deprotonated surface silanol groups at testing pH of 5 when prepared using TEOS (Table 2) (Qiao et al. 2018). Upon surface adsorption of the coumarins to form SiO_2-**3** nanohybrid, the hydrodynamic size of the particles increased from 114.2 to 122.1 nm, and the zeta potential changed from -30.5 to -28.4 mV, a slight increase. Upon the addition of Cu(II) (at the final concentration of 40 µM) to the SiO_2-**3** nanohybrid solution, the zeta potential dropped to − 22.8 mV. As for comparison, when SiO_2 NPs were treated with Cu(II) at the same concentration, the zeta potential displayed an even more obvious change to − 13.2 mV, suggesting significant surface adsorption of Cu(II) on the surface of SiO_2 as expected due to the presence of negatively charged hydroxylate as well as -OH surface groups (Chen et al. 2021). Cu(II) adsorption by SiO_2 surface as a reason behind improved sensing performance as it is another evidence of Cu(II) adsorbing onto SiO_2.

Fluorescence study of coumarin 3 in the absence and presence of Cu(II)

The pH and concentration dependence of the fluorescence properties of the coumarin **3** were studied in aqueous solution to find the optimum conditions for their application for Cu(II) sensing. Fluorescence intensity of the coumarin **3** was studied across the pH range from 3 to 11 (Fig. S11 (a)) showing that, in the range of pH 5–8, the molecule exhibited the highest intensity. However, when fluorescence intensities at concentrations of 0–80 µM dissolved coumarin **3** were recorded (Fig. S11(b)), no significant differences were observed above 40 µM.

Fluorescence titration of **3** (40 µM) with $CuCl_2$ dihydrate (0–80 µM) in DMSO/HEPES buffer (v/v, 1/9) was conducted (Fig. 4) to identify the linear range and limit of detection. Coumarin **3** responded with gradually quenched fluorescence intensities upon addition of increasing amounts of $CuCl_2$ at the emission maximum of 481 nm (λ_{ex} = 435 nm). The fluorescence intensity response of **3** within the range of 0–80 µM of Cu(II) lacked satisfactory linear correlation (R^2 = 0.96, in 0–40 µM range) contrary to the previously published work (Jung et al. 2009).

Table 2 Hydrodynamic size (nm) and zeta potential (mV) of SiO_2 NPs (7.5 mg/L) before and after surface interaction with coumarin **3** (7.5 mg/L) in HEPES buffer (20 mM, pH = 5), and in the absence or presence of Cu(II)(40 µM)

Samples	Size (nm)	Zeta potential (mV)
SiO_2 NPs	114.2	− 30.5 ± 0.5
SiO_2-**3** nanohybrid	122.4	− 28.4 ± 0.2
SiO_2-**3** nanohybrid + Cu(II)	123.1	− 22.8 ± 0.4
SiO_2 NPs + Cu(II)	114.8	− 13.2 ± 0.6

Fluorescence study of SiO_2-3 nanohybrid in the absence and presence of Cu(II)

Fluorescence of the SiO_2 NPs was negligible in HEPES buffer (20 mM, pH = 5, λ_{ex} = 435 nm) (Fig. S12). To find the optimal working parameters, the fluorescence intensity of the SiO_2-**3** nanohybrid was recorded at the excitation wavelength of **3**, 435 nm, and across the pH range of 3–11 (Fig. S13(a)). The highest fluorescence emission intensity occurred at pH 4. In addition, various concentrations of the SiO_2-**3** nanohybrid (50 to 0.5 mg/L) (Fig. S13(b) and (c)) in HEPES buffer were considered. The fluorescence emission intensity of the SiO_2-**3** nanohybrid was highest at 7.5 mg/L.

Although the greatest fluorescence intensity was observed at pH 4, at this pH, SiO_2-**3** nanohybrid does not respond to Cu(II) (Fig. S14). However, at pH 4.5 or 5, the fluorescence quenching of SiO_2-**3** nanohybrid by Cu(II) was more significant. Thus, pH 5 was selected as the working pH in the following studies. The pH dependence of the fluorescence quenching of coumarin **3** by Cu(II) was also assessed (Fig. S15), and similarly, the extent of fluorescence quenching was greater with increasing basicity of the solution in the presence of equal amounts of Cu(II) added.

Fluorescence titration of both **3** (40 µM) and SiO_2-**3** nanohybrid (7.5 mg/L) with $CuCl_2$ (0–260 µM) in HEPES buffer was conducted (Fig. 5). The SiO_2-**3** nanohybrid displayed linear correlation between fluorescence quenching and Cu(II) concentration over the 0.033–55 and 55–260 µM ranges (R^2 = 0.98), though the sensitivities (slope) (inset of Fig. 5) were different for each range. This is a valuable extension of the sensing range when compared to coumarin **3**, especially as the regulatory limit for Cu(II) in drinking water is specified by the Australian Drinking Water

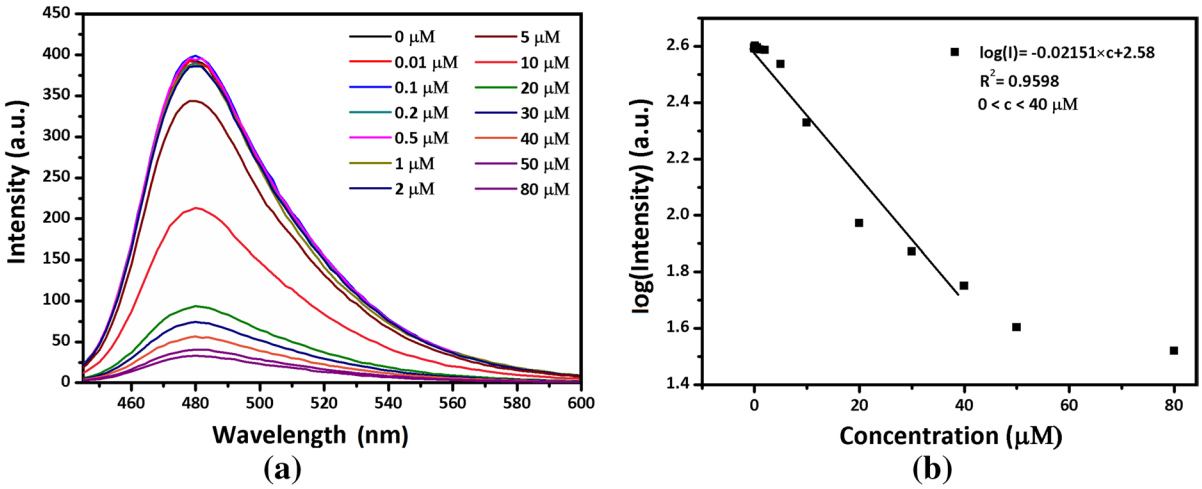

Fig. 4 (**a**) Fluorescence spectra of **3** (40 μM, λ_{ex} = 435 nm) and (**b**) fluorescence intensity changes of **3** with addition of $CuCl_2$ from 0 to 80 μM in HEPES/DMSO buffer (20 mM, pH 5)

Guidelines at 30 μM (NHMRC N 2011) and 10 mg/kg in soil. The LOD was 0.033 μM, tenfold lower than that of coumarin **3** at 0.48 μM.

Interference study of SiO_2-3 nanohybrid

To study the influence of other metal ions on the Cu(II)/SiO_2-**3** nanohybrid interaction, interference study was conducted with a variety of metal ions applied at an excess concentration (200 μM each) to SiO_2-**3** nanohybrid (7.5 mg/L) and Cu(II) (80 μM). Such additional ions were Al(III), Ca(II), Cd(II), Co(II), Fe(III), Mn(II), Pb(II), Hg(II), Ni(II), Zn(II), Mg(II), Cu(I), and Fe(II). Fluorescence emission spectra were examined with and without the addition of Cu(II) (Fig. 6). The measurements indicated no significant interference apart from Fe(III), which means the selectivity of **3** was successfully preserved.

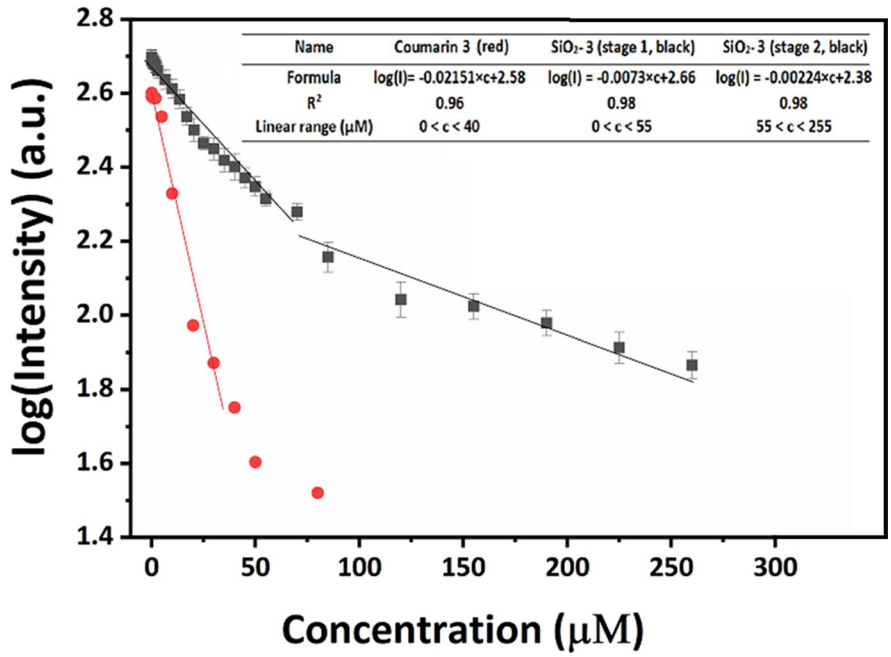

Fig. 5 Fluorescence emission intensity change (λ_{ex} = 435 nm) of coumarin **3** (red, 40 μM) and SiO_2-**3** nanohybrid (black, 7.5 mg/L, n = 3) upon the addition of various concentrations of $CuCl_2$ in HEPES buffer (pH = 5, 20 mM)

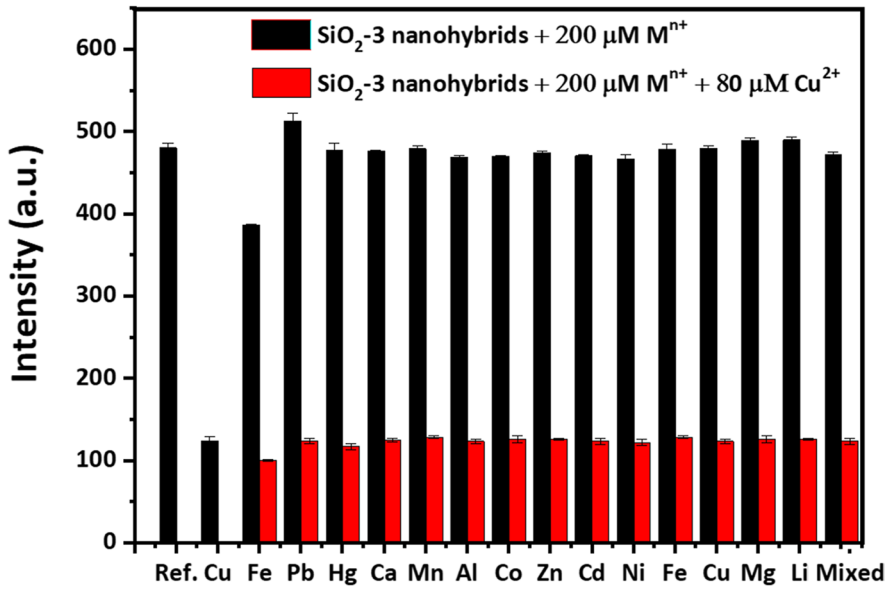

Fig. 6 Fluorescence emission intensities (λ_{ex} = 435 nm) of SiO_2-**3** nanohybrid (7.5 mg/L) in the presence (red bars) and absence (black bars) of Cu(II) (40 μM) when pre-mixed with various cations (200 μM) in HEPES buffer (pH = 5, 20 mM, n = 3)

Cu(II) adsorption by SiO_2 surface as a reason behind improved sensing performance

ICP-OES was employed to determine the amount of Cu(II) adsorbed on both SiO_2 NPs and SiO_2-**3** nanohybrid (both presenting (-OH/-O^- surface groups) using the back-titration procedure described in the "Experiment" section (Table S1). SiO_2 NPs and SiO_2-**3** nanohybrid were used at 15 mg/L, respectively, with Cu(II) added at 9.4 mg/L. ICP-OES results showed the residual Cu(II) in the mother liquor as 7.0 mg/L in both cases. This means the SiO_2 NP has a 2.4 mg/L Cu(II) adsorption. This is slightly lowered when coumarin **3** is adsorbed in SiO_2-**3** nanohybrid at a ~ 4% (weight ratio). Hence, interaction of Cu(II) with both the coumarin **3** and the SiO_2 NP surface results in the less steep slope/increased sensitivity of the sensing observed upon addition of Cu(II) when compared to that of the coumarin **3** itself (Fig. 5). This results in an extended linear detection range of SiO_2-**3** nanohybrid for Cu(II) sensing in the range of 0.033–260 μM. Moreover, approximately tenfold less amount of coumarin **3** was present in the SiO_2-**3** nanohybrid versus when coumarin **3** used alone. This allows for less organic dye to be used while achieving improved applicable sensing range.

Application of SiO_2-3 nanohybrid on real soil samples

Roadside surface soil samples were collected in the western parts of Melbourne, Victoria, Australia (Li et al. 2016). The soil samples were dispersed in water and digested while shaken for 7 days to ensure maximal dissolution of all the soluble metals. The soil samples were analyzed for their Cu content by the industry standard quantification: inductively coupled plasma mass spectrometry (ICP-MS). Next, fluorescence titration using 15 mg/mL SiO_2-**3** nanohybrid (1.5 mL) was conducted at pH 5. Then the soil extracts (1.5 mL) were then merged with the SiO_2-**3** nanohybrid

Table 3 Determination of Cu(II) concentration and recovery values in soil extracts (n = 3 for each sample)

	Cu(II) by ICP-MS (μM)	Fluorescence intensity λ_{em} = 481 nm (a.u.)	Cu(II) by SiO_2-**3** (μM)	Recovery
Sample 1	1.25 ± 0.13	468.47 ± 2.36	1.31 ± 0.02	104.8%
Sample 2	1.38 ± 0.21	468.5 ± 1.72	1.30 ± 0.02	94.2%
Sample 3	1.73 ± 0.27	465.62 ± 1.45	1.69 ± 0.02	97.6%

solution resulting in a concentration of 7.5 mg/mL. The background fluorescence of the soil extracts is shown on Fig. S16. Fluorescence intensities were converted into Cu(II) concentrations based on the titration curves (Fig. 5). The results obtained were then compared against the ICP-MS results. The recovery of Cu(II), directly from the water extract without further sample preparation, was between 105 and 94% for all three soil samples tested (Table 3) (Qian et al. 2019).

Conclusions

SiO_2-**3** nanohybrid was designed, synthesized, characterized, and evaluated for their use for Cu(II) sensing in aqueous media while omitting any organic solvent carrier (required for **3** used alone). SiO_2-**3** nanohybrid exhibited equal selectivity towards Cu(II) in the presence of other multivalent metal ions compared to coumarin **3**. The sensing signal of SiO_2-**3** nanohybrid versus Cu(II) concentration was linear in the range of 0.033–260 µM, which is in good correspondence with the relevant WHO and Australia standards for Cu(II) content in soil and water, and even intra-cellular imaging. This linear sensing range of the nanohybrid was significantly extended when compared to that of **3** (0–20 µM) from µM to nM level. The limit of detection in aqueous media was 0.033 µM, a more than tenfold improvement from LOD 0.48 µM of **3**. SiO_2-**3** nanohybrid also outperforms some of the previously reported surface-modified SiO_2 NP systems used for Cu(II) sensing (Table S2).

The impact of this work is the demonstrated (i) improvement of Cu(II) sensing performance; (ii) use of tenfold reduction amounts of organic molecular probe used when loaded onto the SiO_2 nanoparticles while achieving superior sensing performance; and (iii) omission of organic solvents, when SiO_2-**3** nanohybrid was used and compared to **3** alone. This approach offers reduced cost of synthesis and potentially the amount of (in some cases toxic) organic dye used. SiO_2-**3** nanohybrid was validated on real soil samples against the industry standard ICP-MS technique and showed satisfactory accuracy. Therefore, the concept of SiO_2-**3** nanohybrid offers a convenient and customizable strategy for the use of organic sensing probes in fully aqueous media with the added benefit of improved optical sensing properties, such as linear sensing range and detection limit.

Author contribution

Bin Qian: conceptualization, methodology, formal analysis, writing—original draft, writing—review and editing. Linda Váradi: conceptualization, methodology, writing—original draft, writing—review and editing, supervision. Shamali De Silva: formal analysis. Suzie M Reichman: methodology, supervision. Lei Bao: supervision. Adrian Trinchi: writing—review and editing. Minbo Lan: writing—review and editing. Gang Wei: supervision. Ivan Cole: conceptualization, methodology, writing—review and editing, supervision, funding acquisition.

Acknowledgements Bin Qian would like to show his appreciation to Jo Cosgriff (CSIRO) for her assistance with the NMR and MS analyses, to Paul Morrision who provided the ICP-MS results, and to Winston Liew for ICP-OES results.

Funding Open Access funding enabled and organized by CAUL and its Member Institutions

Declarations

Conflict of interest The authors declare no competing interests.

References

Chen CC, Zhu X, Xu H, Chen F, Ma J, Pan K (2021) Copper adsorption to microplastics and natural particles in seawater: a comparison of kinetics, isotherms, and bioavailability. Environ Sci Tech 55(20):13923–13931

Domaille DW, Zeng L, Chang CJ (2010) Visualizing ascorbate-triggered release of labile copper within living cells using a ratiometric fluorescent sensor. J Am Chem Soc 132(4):1194–1195

Fors BP, Poelma JE, Menyo MS, Robb MJ, Spokoyny DM, Kramer JW et al (2013) Fabrication of unique chemical patterns and concentration gradients with visible light. J Am Chem Soc 135(38):14106–14109

Ge EJ, Bush AI, Casini A, Cobine PA, Cross JR, DeNicol GM et al (2021) Connecting copper and cancer: from transition metal signalling to metalloplasia. Nat Rev Cancer 22:102–113

Geißler D, Antonenko YN, Schmidt R, Keller S, Krylova OO, Wiesner B et al (2005) (Coumarin-4-yl) methyl esters as highly efficient, ultrafast phototriggers for protons and their application to acidifying membrane surfaces. Angew Chem Int Ed 44(8):1195–1198

Grasso GI, Gentile S, Giuffrida ML, Satriano C, Sgarlata C, Sgarzi M et al (2013) Ratiometric fluorescence sensing and cellular imaging of Cu^{2+} by a new water soluble trehalose-naphthalimide based chemosensor. RSC Adv 3(46):24288–24297

Hao X, Xie P, Zhu YG, Taghavi S, Wei G, Rensing C (2015) Copper tolerance mechanisms of Mesorhizobium amorphae and its role in aiding phytostabilization by Robinia pseudoacacia in copper contaminated soil. Environ Sci Tech 49(4):2328–2340

He C, Zhu W, Xu Y, Chen T, Qian X (2009) Trace mercury (II) detection and separation in serum and water samples using a reusable bifunctional fluorescent sensor. Anal Chim Acta 651(2):227–233

He Z, Shentu J, Yang X, Baligar VC, Zhang T, Stoffella PJ (2015) Heavy metal contamination of soils: sources, Indicators and Assessment. J Environ Indicat 99:17–18

Huang J, Gao X, Jia J, Kim JK, Li Z (2014) Graphene oxide-based amplified fluorescent biosensor for Hg^{2+} detection through hybridization chain reactions. Anal Chem 86(6):3209–3215

Jakeria M, Ward L, Cole I (2021) Long term durability studies on the corrosion inhibition effect of 2-mercaptobenzimidazole ($C_3H_4N_2S$) on AA6022: mechanism of film formation and influence of IMPs. Surf Interf 25:101–164

Ji CH, Li JJ, Hou CJ, Huo DQ, Yang M, Zhang L (2017) Mesoporous hollow silica shells modified with functional diamine groups show high-performance absorption capacity and selective colorimetric response to copper ions in aqueous solutions. Sensor Actuat B Chem 240:718–725

Jung HS, Kwon PS, Lee JW, Kim JI, Hong CS, Kim JW et al (2009) Coumarin-derived Cu^{2+}-selective fluorescence sensor: synthesis, mechanisms, and applications in living cells. J Am Chem Soc 131(5):2008–2012

Kraljević TG, Harej A, Sedić M, Pavelić SK, Stepanić V, Drenjančević D et al (2016) Synthesis, in vitro anticancer and antibacterial activities and in silico studies of new 4-substituted 1, 2, 3-triazole–coumarin hybrids. Euro J Med Chem 124:794–808

Li P, Lang M, Wang XX, Zhang TL (2016) Sorption and desorption of copper and cadmium in a contaminated soil affected by soil amendments. Clean-Soil, Air, Water 44(11):1547–1556

Li H, Sun X, Zheng T, Xu Z, Song Y, Gu X (2019) Coumarin-based multifunctional chemosensor for arginine/lysine and Cu^{2+}/Al^{3+} ions and its Cu^{2+} complex as colorimetric and fluorescent sensor for biothiols. Sensor Actuat B Chem 279:400–409

Lin W, Huang YW, Zhou XD, Ma Y (2006) In vitro toxicity of silica nanoparticles in human lung cancer cells. Tox Appl Pharm 217(3):252–259

Meiling W, Guowen M (2017) Fluorophores-modified nanomaterials for trace detection of polychlorobiphenyls and heavy metal ions. Sensor Actuat B Chem 243:1137–1147

NHMRC N (2011) Australian drinking water guidelines. Commonwealth of Australia.

Nielsen AT, Houlihan WJ (2004) The Aldol Condensation Organic Reactions 16:1–438

Peng J, Li J, Xu W, Wang L, Su D, Teoh CL et al (2018) Silica nanoparticle-enhanced fluorescent sensor array for heavy metal ions detection in colloid solution. Analy Chem 90(3):1628–1634

Qian B, Váradi L, Trinchi A, Reichman SM, Bao L, Lan M et al (2019) The design and synthesis of fluorescent coumarin derivatives and their study for Cu^{2+} sensing with an application for aqueous soil extracts. Molecules 24(19):3569

Qiao Y, Liu C, Zheng X (2018) Enhancing the quantum yield and Cu^{2+} sensing sensitivity of carbon dots based on the nano-space confinement effect of silica matrix. Sensor Actuat B Chem 259:211–218

Ramdass A, Sathish V, Babu E, Velayudham M, Thanasekaran P, Rajagopal S (2017) Recent developments on optical and electrochemical sensing of copper (II) ion based on transition metal complexes. Coordin Chem Rev 343:278–307

Seeley M, Wells CS, Wannamaker EJ, Mattuck RL, Ren SJ, Beck D (2013) Determining soil remedial action criteria for acute effects: the challenge of copper. Reg Tox Pharm 65(1):47–59

Seo KD, Song HM, Lee MJ, Pastore M, Anselmi C, De Angelis F et al (2011) Coumarin dyes containing low-band-gap chromophores for dye-sensitised solar cells. Dye Pigment 90(3):304–310

Sivaraman G, Iniya M, Anand T, Kotla NG, Sunnapu O, Singaravadivel S et al (2018) Chemically diverse small molecule fluorescent chemosensors for copper ion. Coordin Chem Rev 357:50–104

Stöber W, Fink A, Bohn E (1968) Controlled growth of monodisperse silica spheres in the micron size range. J Colloid Interf Sci 26(1):62–69

Tang M, Harmon S, Nadagouda MN, Lytle DA (2021) Quartz crystal microbalance with dissipation: a new approach of examining corrosion of new copper surfaces in drinking water. Environ Sci Tech 55(16):11265–11273

Tham TDQ, Chung I, Kim T, Kang J, Tan MM, Kim Dung NT, et al. et al (2020)Preparation, stabilization and characterization of 3-(methacryloyloxy) propyl trimethoxy silane modified colloidal nanosilica particles. Colloid Surf A 585:124066

Wang Y, Zhang C, Chen X, Yang B, Yang L, Jiang C et al (2016) Ratiometric fluorescent paper sensor utilizing hybrid carbon dots–quantum dots for the visual determination of copper ions. Nanoscale 8(11):5977–5984

Zhang H, Li Y, Liu X, Liu P, Wang Y, An T et al (2014) Determination of iodide via direct fluorescence quenching at nitrogen-doped carbon quantum dot fluorophores. Environ Sci Tech Let 1(1):87–91

Zhang Z, Liu Y, Wang E (2019) A highly selective "turn-on" fluorescent probe for detecting Cu^{2+} in two different sensing mechanisms. Dye Pigment 163:533–537

Zhu A, Qu Q, Shao X, Kong B, Tian Y (2012) Carbon-dot-based dual-emission nanohybrid produces a ratiometric fluorescent sensor for in vivo imaging of cellular copper ions. Angew Chem Int Ed 51(29):7185–7189

Zhuravlev LT (2000) The surface chemistry of amorphous silica. Zhuravlev Model Colloid Surf A 173(1):1–38